



# A controllable hydrothermal fabrication of hierarchical ZnO microstructures and its gas sensing properties

Xiao Qu<sup>1</sup> · Rong Yang<sup>1</sup> · Ye Zhao<sup>1</sup> · Fan Tong<sup>1</sup> · Mao-Hua Wang<sup>1</sup>

Received: 10 November 2017 / Accepted: 22 December 2017 / Published online: 16 January 2018  
© Springer Science+Business Media, LLC, part of Springer Nature 2018

## Abstract

In this paper, rod-flower like ZnO hierarchical microstructures with high uniformity are synthesized from the thermal decomposition of  $\text{Zn}(\text{NH}_3)_4^{2+}$  precursors, which are prepared via a surfactant-assisted hydrothermal process. The as-synthesized hierarchical ZnO microstructure is assembled from columnar nanorods, and the measured length to diameter ratio of the nanorod is about 20. The morphology of the hierarchical ZnO microstructure can be tailored by varying hydrothermal conditions, e.g., hydrothermal temperature, reaction time, concentration of  $\text{Zn}^{2+}$  and zinc salts. Moreover, based on the experimental results, the possible reaction mechanism for the growth of the as-synthesized hierarchical ZnO microstructures is also discussed in detail, and the  $\text{Zn}^{2+}$  concentration was found to be a crucial role in the formation and nucleation of the rod flower-like microstructures. In addition, the gas sensing test demonstrates that the sensors based on hierarchical ZnO microstructures exhibits excellent gas sensing properties due to its unique architecture.

## 1 Introduction

Micro/nanostructures with three-dimensional (3D) hierarchical structures have been extensively studied owing to their attractive physicochemical properties and potential applications. Zinc oxide (ZnO), as a typical n-type wide band gap semiconductor ( $E_g = 3.37$  eV, at 300 K) and large exciton binding energy (60 meV) at room temperature [1], which exhibits outstanding catalytic, electrical and sensing properties, has wide applications in solar cells [2], photocatalysts [3], field-effect transistors [4] and sensors [5, 6]. The enormous attention in ZnO is due to its distinct construction and unique capability. In recent years, ZnO micro/nanostructures with diverse morphologies such as nanowires (1D) [7], nanosheets (2D) [8], nanocubes (3D) [9] and hierarchical architectures [10] have been explored by different synthetic routes. Among these unique architectures, hierarchical structures assembled from 1D and 2D nanoscale building blocks have attracted tremendous attention for their special ability of possessing structure-dependent performance [1]. Controllable synthesis of size, morphology and crystallization of hierarchical ZnO micro/nanostructures is highly

desirable for a latent wide range of applications. Meanwhile, a controllable fabrication of 3D hierarchical architectures from micro/nano-scale building blocks still preserves a challenge owing to the strict demand for exact control of crystal growth process.

Up to date, substantial efforts have been dedicated to fabricate 3D hierarchical ZnO micro/nanostructures, the common synthetic strategies such as chemical vapor deposition (CVD) [11], chemical bath deposition (CBD) [12], electrodeposition [13], hydrothermal method [14], thermal evaporation [15] and so on. Hieu et al. [16] described the fabrication of urchin-like ZnO hollow hemisphere through the sputter deposition. Hu et al. [17] reported the solution-controlled self-assembly of ZnO nanorods into hollow microspheres via the hydrothermal process. Wang et al. [18] reported the synthesis of tower-like ZnO structures by a simple carbon thermal reduction method. Among these ways, the hydrothermal method has been confirmed to be a valid and widely applied technique to prepare hierarchical ZnO architectures [19, 20].

In this work, we report a facile approach to synthesize 3D hierarchical ZnO microstructures via a hydrothermal process. The unique constructions of the hierarchical ZnO microstructures provide extreme potential for gas sensing application. The plausible reaction mechanism for the growth of hierarchical ZnO microstructures is also proposed.

✉ Mao-Hua Wang  
1447814890@qq.com

<sup>1</sup> School of Petrochemical Engineering, Changzhou University, Changzhou 213164, People's Republic of China

## 2 Experimental section

### 2.1 Chemicals and preparation

All of the reagents used were analytic grade and without further purification. In a typical process, the  $\text{Zn}(\text{NH}_3)_4^{2+}$  precursor solution can be fabricated by mixing 0.5 M  $\text{ZnAc}_2 \cdot 2\text{H}_2\text{O}$  solution and fresh ammonia (volume ratio is 1:1, pH ~ 10). Then, 4 ml  $\text{Zn}(\text{NH}_3)_4^{2+}$  precursor solution was added to 44 ml deionized water (containing 0.5 g of PEG6000) to form a suspension under vigorous stirring. Afterwards, the mixture was transferred to a 100 ml Teflon-lined stainless steel autoclave, and maintained at 180 °C for 12 h. Following, the autoclave was cooled down to room temperature naturally, the white precipitate was collected by centrifugation, washed with distilled water and ethanol several times, and finally dried at 80 °C for further characterization.

### 2.2 Characterization

The as-fabricated products were characterized by field-emission scanning electron microscopy (FESEM, JEOL JSM-6360LA, Japan) and X-ray diffraction (XRD; Rigaku D/MAX-YA). Gas-sensing properties toward *n*-butanol were measured using a static system controlled by a computer under laboratory conditions. The gas response of sensor was defined as  $R_a/R_g$ , where  $R_a$  is the resistance in ambient air and  $R_g$  is the resistance in test gas atmosphere.

### 2.3 Sensor fabrication and test

The as-synthesized ZnO microstructures were mixed with ethanol and ground. And then, polyethylene glycol 600 (PEG600) as a binder, was added to the mixture to form a paste. The paste was coated on an alumina substrate (20mm × 10mm × 0.635 mm) with 14 pairs of Au interdigitated electrodes (electrodes width and distance: 0.15 mm) to form a sensing film, then the substrate coated ZnO products were dried at 80 °C for 2 h. Subsequently, the substrate was sintered at 450 °C for 30 min.

## 3 Results and discussion

### 3.1 Morphology and phase structure analysis

A low magnification FESEM image (Fig. 1a) shows that the products consist of large-scaled, uniform, rod flower-like architectures with an average diameter of ~5 μm. Figure 1b, c are the magnified FESEM images of two individual hierarchical ZnO microstructures marked by white boxes in Fig. 1a, which reveal the detailed features of two different aggregation patterns. The medium magnification view in Fig. 1b clearly displays that the architecture exhibits a structural symmetry [9]. Interestingly, the two different patterns are composed of many nanorods, and each nanorod has a prismatic shaft and a sharp-like end. Figure 1d shows the typical XRD pattern, all of the diffraction peaks can be indexed to the hexagonal ZnO structure with lattice consists

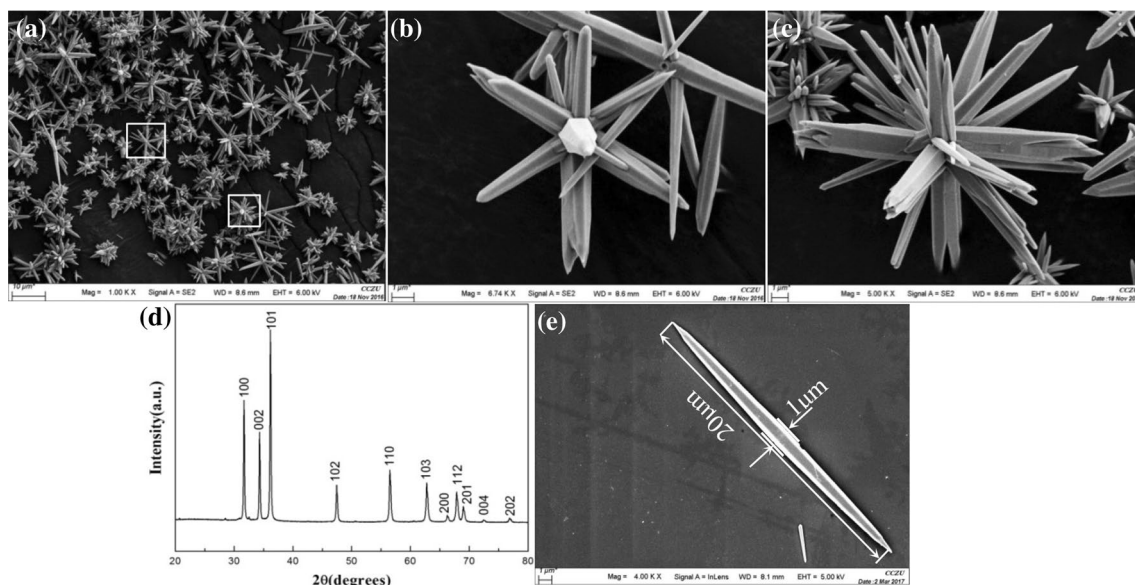


**Fig. 1** **a** Low magnification view of the products; **b**, **c** the magnified images of two individual ZnO marked with a white box in **a**; **d** XRD pattern; **e** the individual ZnO microrod

of  $a = 3.249 \text{ \AA}$  and  $c = 5.206 \text{ \AA}$ , which matched with the standard XRD database (JCPDS Card No. 36-1451). No diffraction peaks of any impurities were observed, indicating the well crystallization. Figure 1e shows an individual ZnO microrod of this as-prepared pattern with a length to diameter ratio of 20, which the length and diameter of ZnO microrod are approximately 20 and 1  $\mu\text{m}$ , respectively. From the images, it can be observed that the surface of microrod is very rough.

### 3.2 Influence of the molar concentration of $\text{Zn}^{2+}$

In addition, the concentration of  $\text{Zn}^{2+}$  plays a crucial role in the morphology of the products. Figure 2a–c shows the FESEM of the samples obtained at 180 °C for 12 h under different molar concentrations of  $\text{Zn}^{2+}$ . When the concentration of  $\text{Zn}^{2+}$  is as low as 0.25 M (shown in Fig. 2a), only single nanorods and several branches on the column-like facets of primary rod can be observed, the branches have an average diameter of  $\sim 500 \text{ nm}$  and the primary rods have an average diameter of  $\sim 1 \mu\text{m}$ . After increasing the concentration to 0.75 M, many branches grow from the middle part of the primary rods, almost all of the primary rods and branches aggregate into 3D hierarchical microstructures (shown in Fig. 2b). As the concentration is further increased to 1 M (Fig. 2c), there are more and more branches growing from the middle part of the primary rods, the hierarchical ZnO microstructures are composed of bigger cone-like rods with more rough surfaces and smaller prismatic shaft, it indicates

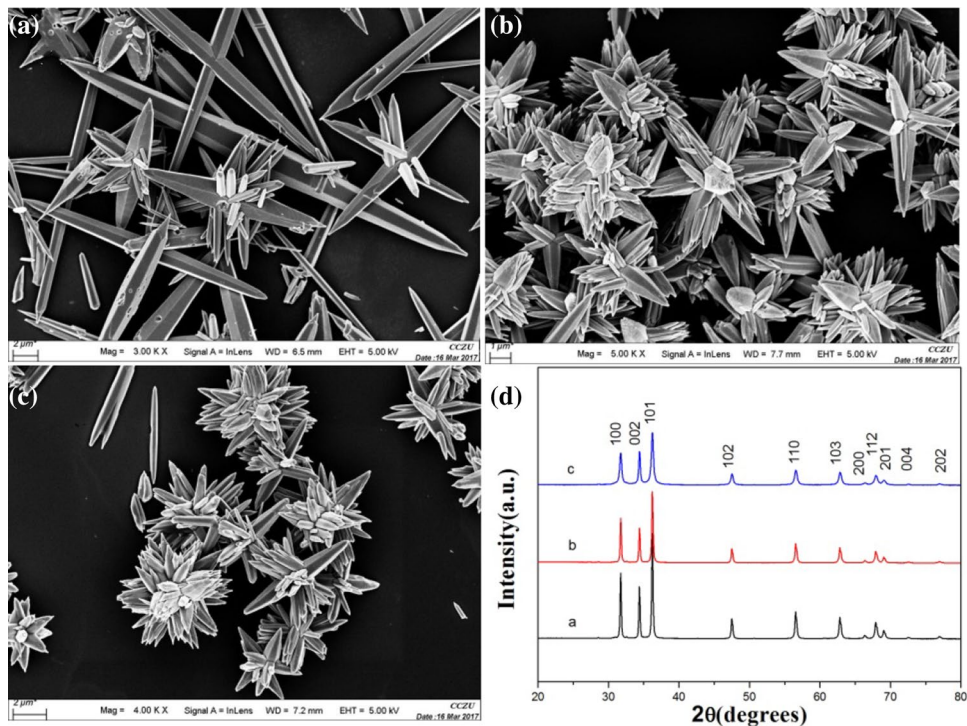
that the branches have an intense trend to grow from the middle part of the column-like facets of the primary rods. The corresponding XRD patterns of the samples synthesized at different concentration of  $\text{Zn}^{2+}$  are shown in Fig. 2d. The obtained products (Fig. 2b, c) display a low diffraction peak owing to the existence of poor crystallization, but sample (c) shows the intensity of (002) peak is stronger. However, it can be noticed that the XRD pattern of sample (a) shows relatively stronger diffraction peak compared to the sample (b and c), and its intensity decreases with the appearance of ZnO branches.

### 3.3 Gas sensing properties

A lot of studies proved that hierarchical structures are excellent materials for applications in gas sensor [21]. Furthermore, the complex hierarchical structures can provide high surface areas, which are good for the adsorption of gas molecule on sensor materials. In this study, the gas sensing performance of the hierarchical ZnO microstructures was investigated toward *n*-butanol.

Figure 3a shows the response of the sensor to 100 ppm *n*-butanol as a function of the testing temperature ranging from 200 to 350 °C. It can be observed that the maximum response was 32.4 at the optimum operation temperature of 275 °C. The response of the sensor to a wide range of concentration of *n*-butanol at 275 °C, as shown in Fig. 3b. According to curve, the responses sharply increased with increasing the gas concentration (range from 40 to

**Fig. 2** FESEM images of the samples synthesized at different concentrations of  $\text{Zn}^{2+}$ : **a** 0.25 M, **b** 0.75 M, **c** 1 M and **d** corresponding XRD patterns of the sample **a**, **b** and **c**



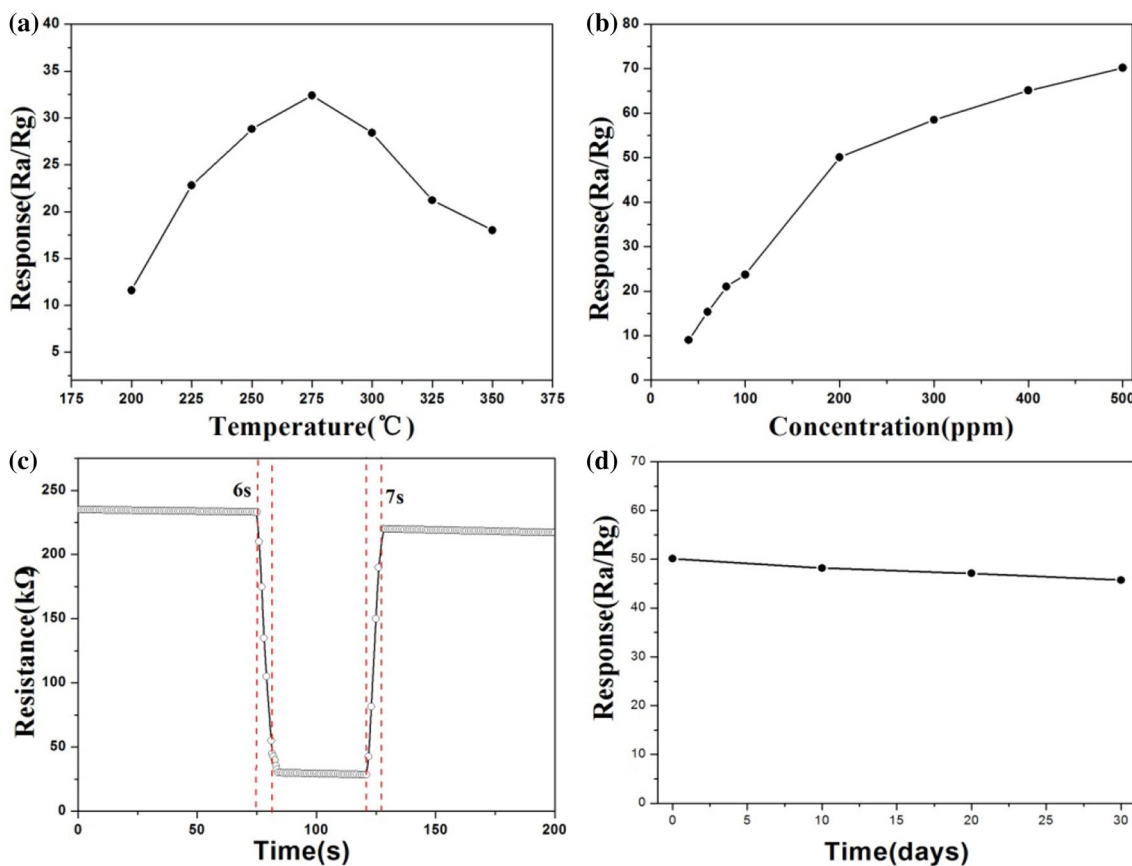


**Fig. 3** **a** The sensor response to 100 ppm *n*-butanol at different operating temperatures; **b** response of the sensor to different concentrations of *n*-butanol at 275 °C; **c** response and recovery curves

of the ZnO microstructures to 100 ppm *n*-butanol at 275 °C; **d** The long-term stability of hierarchical ZnO microstructures to 200 ppm *n*-butanol at 275 °C

100 ppm). As the concentrations of *n*-butanol increased (above 300 ppm), the responses increased slightly, indicating that the sensor tended to saturation gradually. Figure 3c shows the typical dynamical curve of the sensor to 100 ppm *n*-butanol at 275 °C. It can be seen that the sensor exhibited fast response and recovery, as showed by rapid changes in resistance, with a response and recovery time of 6 and 7 s as marked in the figure, respectively. In order to investigate the stability of the sensor based on hierarchical ZnO structures, the gas sensing measurement are repeated over a period of 30 days. The response of sensor exhibits a slightly decrease after 30 days (shown in Fig. 3d), indicating the excellent stability of the as-synthesized ZnO microstructures.

### 3.4 Influence of hydrothermal conditions

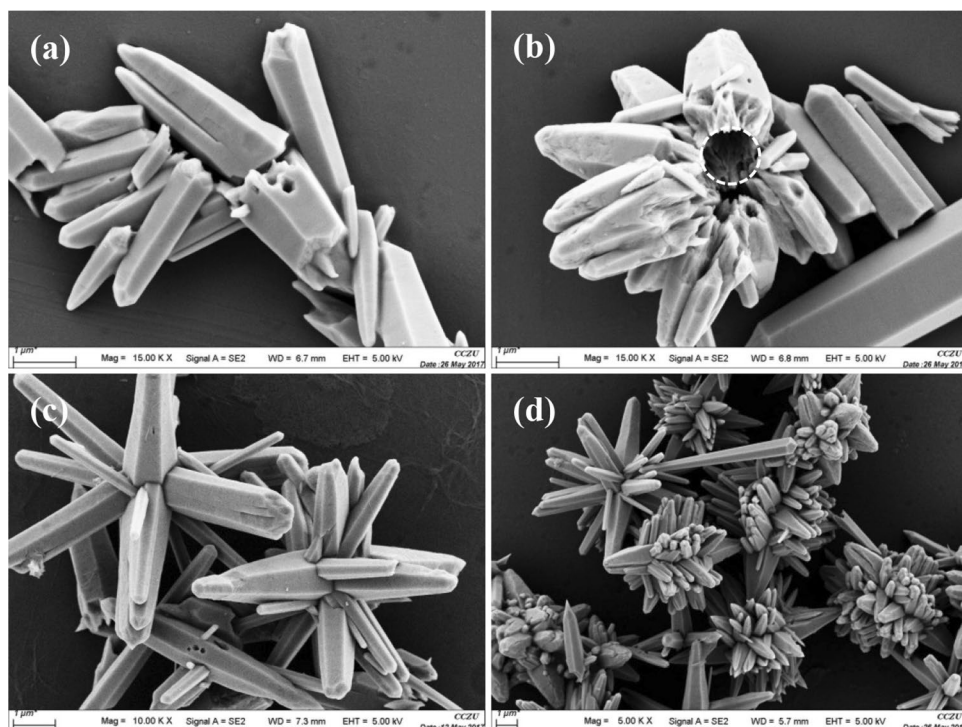
To reveal the effect of the reaction time on the morphology evolution of hierarchical ZnO microstructures, time-dependent experiments were carried out and the ZnO products obtained with different reaction times from 10 min to 4 h, as shown in Fig. 4. When the hydrothermal time was 10 min,

only scattered columnar nanorods could be observed and the products were irregular shape. While the reaction time was expended to 30 min, some rods began to be assembled in an orderly manner. Interestingly, it can be noticed that space existed in the interior of the rod, which marked with a white circle in Fig. 4b. As the reaction time prolonged to 2 h, some nanorods grew from the column-like facets of the larger branches and assembled in an emanative way to form rod-flower like shape, as shown in Fig. 4c. With increasing the time to 4 h, the rods on the columnar facets of the branches tended to be denser and the hierarchical architectures were composed of smaller prism-like rods.

To investigate the morphologies of ZnO structures changing with different reaction temperature, experiments are carried out by varying the hydrothermal temperature while the other conditions remaining unchanged. When the temperature was as low as 90 °C, a bit of scattered primary nanorods existed and the rod flower-like architectures cannot be observed, as shown in Fig. 5a, b. As the temperature reached to 120 °C, some nanorods began to aggregate with each other through the Ostwald ripening process, moreover,



**Fig. 4** SEM images of ZnO microstructures with different reaction times at 180 °C: **a** 10 min, **b** 30 min, **c** 2 h, and **d** 4 h



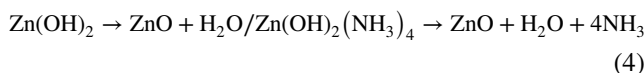
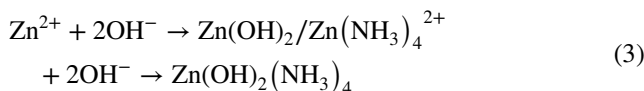
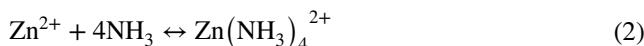
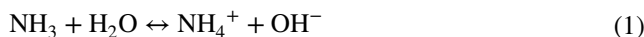
these primary nanorods grow larger and longer due to a faster crystal growth rate (shown in Fig. 5c, d). With increasing the hydrothermal temperature to 150 °C, there are many radiation-like branches growing from the middle trunk of the primary nanorods, the hierarchical ZnO structures consist of prismatic rods are formed gradually, which indicates the secondary rods show a stronger trend to grow from the column facet of the skeleton.

### 3.5 Influence of zinc source

In addition to hydrothermal temperature, reaction time, the crystal formation and the morphology development of ZnO microstructures were highly relied on counter-ion of  $Zn^{2+}$ , according to the previous report [22]. In the work, the effects of different zinc salts on the growth of hierarchical ZnO microstructures were researched by choosing the  $Zn(NO_3)_2 \cdot 6H_2O$ ,  $ZnCl_2$ , and  $ZnSO_4 \cdot 7H_2O$  as zinc source, respectively, while the other conditions maintaining unchanged, as shown in Fig. 6. Obviously, when used the above three types of zinc salts as the zinc source, the morphologies of the obtained ZnO microstructures were strongly different from that shown in Fig. 1. Although the ZnO products were chiseled displayed rod-flower like structures, the nanorods of the synthesized pattern were shorter and denser. The results demonstrated that zinc salts types played a crucial role in the nucleation and formation of hierarchical ZnO microstructures under hydrothermal circumstance.

### 3.6 Reaction mechanism

On the basis of the results, the detailed reactions of ZnO crystallization process in alkaline condition are as follows:



Hydroxy complex such as  $Zn(NH_3)_4^{2+}$ ,  $Zn(OH)_2$  and  $Zn(OH)_2(NH_3)_4$  are dominant in alkaline solution and it is speculated that the dehydration process occurred in this condition. Firstly,  $Zn^{2+}$  ions are released by the hydrolysis of  $ZnAc_2 \cdot 2H_2O$ , when ammonia is added into the solution,  $Zn^{2+}$  easily react with  $OH^-$  to form  $Zn(OH)_2$  precipitate and  $Zn(OH)_2(NH_3)_4$  complex. Afterwards, with the decomposition of  $Zn(OH)_2$  or  $Zn(OH)_2(NH_3)_4$ , ZnO nanoparticles are generated and followed by a growth process. Subsequently,  $Zn(NH_3)_4^{2+}$  generates a large quantity of growth units around ZnO nuclei, leading to faster growth kinetics [23]. In addition, ZnO multipod structures consist of several nanorods united at a common base, and a large

**Fig. 5** FESEM images of ZnO microstructures synthesized at different reaction temperatures: **a, b** 90 °C, **c, d** 120 °C, **e, f** 150 °C

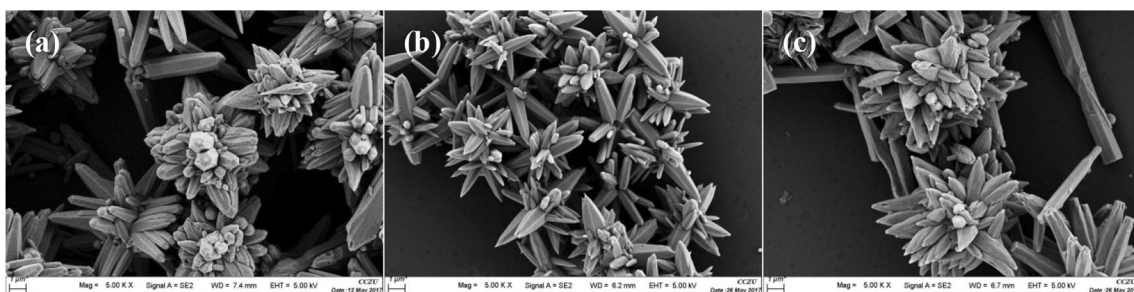
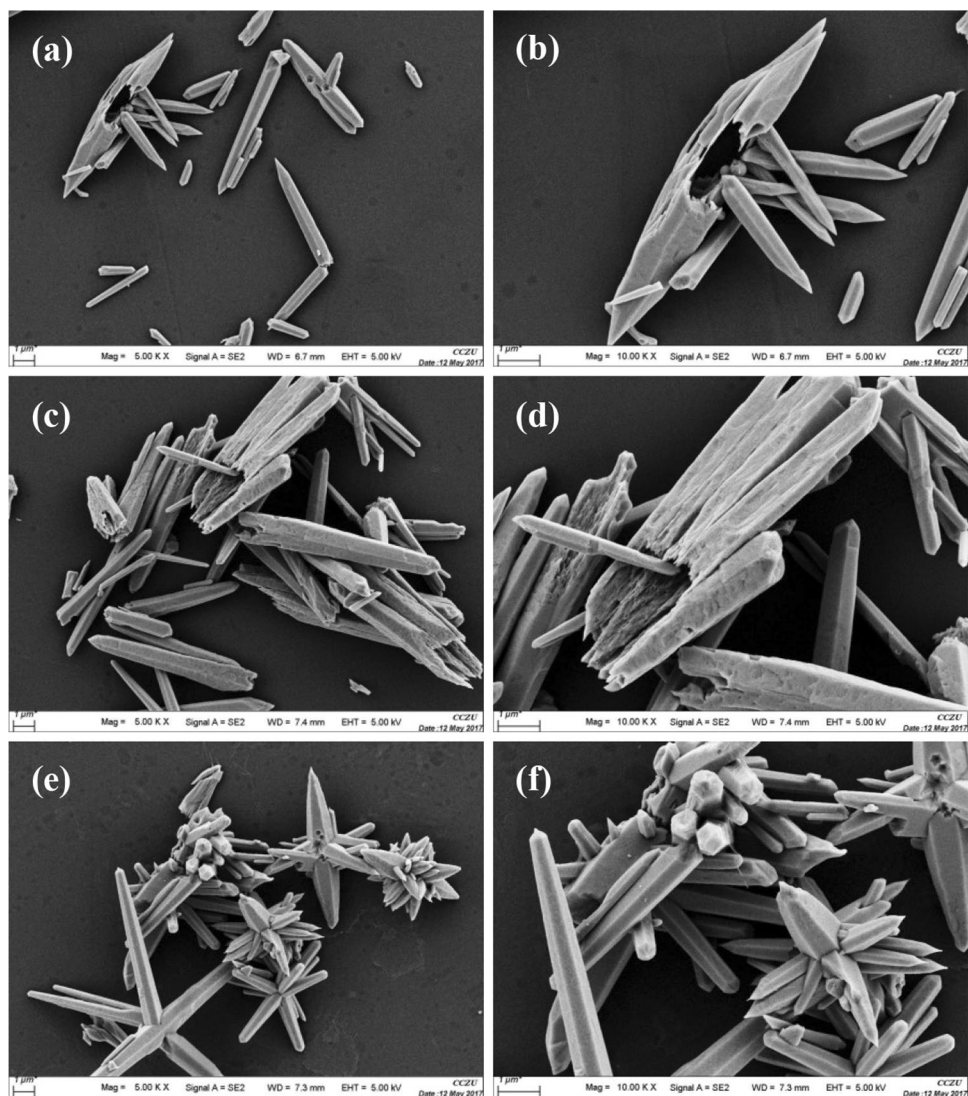


**Fig. 6** SEM images of the ZnO microstructures obtained from different zinc salts: **a**  $\text{Zn}(\text{NO}_3)_2 \cdot 6\text{H}_2\text{O}$ ; **b**  $\text{ZnCl}_2$ ; **c**  $\text{ZnSO}_4 \cdot 7\text{H}_2\text{O}$

amount of growth units  $\text{Zn}(\text{NH}_3)_4^{2+}$  and fast growth kinetics result in the formation of rod flower-like shape. During the process, the addition of PEG in the hydrothermal

system will modify the growth of the ZnO crystal, ZnO nanoparticles nucleate and oriented growth into nanorods via the Ostwald ripening process under the assistance of

PEG, which owing to the driving force of reducing the surface energy [24].

## 4 Conclusion

In summary, 3D hierarchical ZnO microstructures with high uniformity are synthesized via a simple hydrothermal with PEG-assisted. On the basis of detailed morphology study on the ZnO architectures, 3D hierarchical ZnO microstructures are assembled from many nanorods, the measured length and diameter of the nanorod is about 20  $\mu\text{m}$  and 200–500 nm, respectively. It is worth noticing that concentration of  $\text{Zn}^{2+}$  plays a crucial role in the formation process of ZnO architectures. Moreover, the gas-sensing tests indicate that the hierarchical ZnO microstructures have fast response and recovery to *n*-butanol, demonstrating the promising applications in *n*-butanol sensor.

**Acknowledgements** This work was financially supported by Changzhou Science, Technology Innovation Project, Production-teaching-research project of Changzhou university institute of Huaide and 2016 Research and Innovation Project for College Graduates of Jiangsu Province.

## References

1. T. Ichikawa, S. Shiratori, *Inorg. Chem.* **50**, 999–1004 (2011)
2. R. Krishnapriya, S. Praneetha, A.V. Murugan, *New J. Chem.* **40**, 5080–5089 (2016)
3. H.Y. Sun, Y.L. Yu, J. Luo, M. Ahmad, J. Zhu, *CrystEngComm* **14**, 8626–8632 (2012)
4. S. Thiemann, M. Gruber, I. Lokteva, J. Hirschmann, M. Halik, J. Zaumseil, *Appl. Mater. Interfaces* **5**, 1656–1662 (2013)
5. J. Li, H.Q. Fan, X.H. Jia, *J. Phys. Chem. C* **114**, 14684–14691 (2010)
6. J.Y. Liu, M.J. Dai, T.S. Wang, P. Sun, X.S. Liang, G.Y. Lu, K. Shimano, N. Yamazoe, *Appl. Mater. Interfaces* **8**, 6669–6677 (2016)
7. J.-H. Park, J.-H. Lee, *Sens. Actuators B* **136**, 151–157 (2009)
8. C.-S. Moon, H.-R. Kim, G. Auchterlonie, J. Drennan, J.-H. Lee, *Sens. Actuators B* **131**, 556–564 (2008)
9. X.F. Chu, D.L. Jiang, C.M. Zheng, *Sens. Actuators B* **123**, 793–797 (2007)
10. J.Y. Lao, J.G. Wen, Z.F. Ren, *Nano Lett.* **2**, 1287–1291 (2002)
11. X.W. Lou, L.A. Archer, Z.C. Yang, *Adv. Mater.* **20**, 3987–4019 (2008)
12. H.H. Wang, C.S. Xie, *J. Cryst. Growth* **291**, 187–195 (2006)
13. Q. Hou, L.Q. Zhu, H.L. Chen, H.C. Liu, W.P. Li, *Electrochim. Acta* **78**, 55–64 (2012)
14. Q. Zhou, W.G. Chen, J. Li, C. Tang, H. Zhang, *Mater. Lett.* **161**, 499–502 (2015)
15. C. Xu, G. Xu, Y. Liu, G.A. Wang, *Solid State Commun.* **122**, 175–179 (2002)
16. H.N. Hieu, N.M. Vuong, H. Jung, D.M. Jang, D.J. Kim, H. Kim, S.K. Hong, *J. Mater. Chem.* **22**, 1127–1134 (2012)
17. P. Hu, X. Zhang, N. Han, W.C. Xiang, Y.B. Cao, F.L. Yuan, *Cryst. Growth Des.* **11**, 1520–1526 (2011)
18. F.F. Wang, L. Cao, A.L. Pan, R.B. Liu, X. Wang, X. Zhu, S.Q. Wang, B.S. Zou, *J. Phys. Chem. C* **111**, 7655–7660 (2007)
19. D.F. Zhang, L.D. Sun, J. Zhang, Z.G. Yan, C.H. Yan, *Cryst. Growth Des.* **8**, 3609–3615 (2008)
20. W.W. Wang, Y.J. Zhu, L.X. Yang, *Adv. Funct. Mater.* **17**, 59–64 (2007)
21. Z. Jing, J. Zhan, *Adv. Mater.* **20**, 4547–4551 (2008)
22. K. Kakiuchi, E. Hosono, T. Kimura, H. Imai, S. Fujihara, *J. Sol Gel Sci. Technol.* **39**, 63–72 (2006)
23. R. Krishnapriya, S. Praneetha, A.V. Murugan, *CrystEngComm* **17**, 8353–8367 (2015)
24. Y.G. Sun, R.J. Zou, W.Y. Li, Q.W. Tian, J.H. Wu, Z.G. Chen, J.Q. Hu, *CrystEngComm* **13**, 6107–6113 (2011)